Cancer Research

Chromatin-Remodeling Complex SWI/SNF Controls Multidrug Resistance by Transcriptionally Regulating the Drug Efflux Pump ABCB1

Ramin Dubey[1,2], Andres M. Lebensohn[1,2], Zahra Bahrami-Nejad[3], Caleb Marceau[4], Magali Champion[5], Olivier Gevaert[5], Branimir I. Sikic[2], Jan E. Carette[4], and Rajat Rohatgi[1,2]

Abstract

Anthracyclines are among the most effective yet most toxic drugs used in the oncology clinic. The nucleosome-remodeling SWI/SNF complex, a potent tumor suppressor, is thought to promote sensitivity to anthracyclines by recruiting topoisomerase IIa (TOP2A) to DNA and increasing double-strand breaks. In this study, we discovered a novel mechanism through which SWI/SNF influences resistance to the widely used anthracycline doxorubicin based on the use of a forward genetic screen in haploid human cells, followed by a rigorous single and double-mutant epistasis analysis using CRISPR/Cas9-mediated engineering. Doxorubicin resistance conferred by loss of the SMARCB1 subunit of the SWI/SNF complex was caused by transcriptional upregulation of a single gene, encoding the multidrug resistance pump ABCB1. Remarkably, both ABCB1 upregulation and doxorubicin resistance caused by SMARCB1 loss were dependent on the function of SMARCA4, a catalytic subunit of the SWI/SNF complex. We propose that residual SWI/SNF complexes lacking SMARCB1 are vital determinants of drug sensitivity, not just to TOP2A-targeted agents, but to the much broader range of cancer drugs effluxed by ABCB1. *Cancer Res; 76(19); 5810–21. ©2016 AACR.*

Introduction

Anthracyclines are used to induce regressions in multiple disseminated neoplasms in both adults and children, including acute leukemias, breast and ovarian cancers, bone and soft tissue sarcomas, Hodgkin's disease, and malignant lymphomas. The most commonly used anthracyclines (doxorubicin, daunorubicin, idarubicin, and epirubicin) trap or "poison" a covalent reaction intermediate between DNA and tyrosine residues in type II topoisomerases, eventually causing double-strand breaks (DSB) and cell death (1, 2). The DNA cleavage activity of Topoisomerase IIα (TOP2A) is thought to be required for anthracycline toxicity; indeed, lower TOP2A levels are associated with greater resistance (3, 4). Recent studies have proposed that the SWI/SNF chromatin-remodeling complex recruits TOP2A to DNA, thereby promoting anthracycline-induced DSBs and cell death (5, 6). A second mechanism of resistance to anthracyclines (and many other chemotherapeutic drugs) is overexpression of *ABCB1*, which encodes an ATP-dependent promiscuous drug efflux pump also known as the Multidrug Resistant (MDR1) pump or P-glycoprotein (PgP) pump (7).

A forward genetic screen revealed 35 loci associated with sensitivity to doxorubicin, a commonly used anthracycline. Top hits from this screen included many chromatin regulators, including five subunits of the nucleosome-remodeling SWI/SNF complex and two subunits of the histone acetylating STAGA complex. In particular, we found that the chromatin remodeling SWI/SNF complex regulates expression of ABCB1, entirely explaining the source of resistance seen in cells lacking particular subunits of this complex. It follows from these findings that targeting chromatin regulators, a recent focus of therapeutic development due to their oncogenic role in many tumors, may also modulate the sensitivity of these tumors to chemotherapeutic agents.

Materials and Methods

Cell lines and constructs

The Hap1 cell line (8) was kindly provided by Dr. Thijn Brummelkamp, Netherlands Cancer Institute. The 293FT cell line used to generate high-titer lentiviruses was obtained from Thermo Fisher Scientific; the A549, PC3, MDA-MB-361, HCC-1954, and NCI-H1650 cell lines were purchased from the ATCC, where they were validated by short tandem repeat profiling, and used at passage numbers <5. The KOPN8 cell line was a generous gift from

[1]Department of Biochemistry, Stanford University School of Medicine, Stanford, California. [2]Division of Oncology, Department of Medicine, Stanford University School of Medicine, Stanford, California. [3]Department of Chemical and Systems Biology, Stanford University School of Medicine, Stanford, California. [4]Department of Microbiology and Immunology, Stanford University School of Medicine, Stanford, California. [5]Stanford Center for Biomedical Informatics Research, Dept. of Medicine, Stanford, California.

Note: Supplementary data for this article are available at Cancer Research Online (http://cancerres.aacrjournals.org/).

R. Dubey and A.M. Lebensohn contributed equally to this article.

Corresponding Authors: R. Rohatgi, Stanford University School of Medicine, 279 W. Campus Drive, Room B435, Stanford, CA 94305. Phone: 650-387-5666; Fax: 650-723-6783; E-mail: rrohatgi@stanford.edu; or J.E. Carette, Stanford University, Department of Microbiology and Immunology, 299 Campus Drive, Room D345, Stanford, CA 94305. Phone: 650-725-4468; Fax: 650-725-7282; E-mail: carette@stanford.edu

doi: 10.1158/0008-5472.CAN-16-0716

Professor Michael Cleary, Stanford University. The SNU-349 cell line was obtained from Korean Cell Line Bank. The Phoenix-Ampho cell line used for retrovirus production was purchased from Allele Biotechnology.

Null alleles for genes were constructed using the CRISPR/Cas9 system. For Hap1 cells, the oligos encoding the guide RNAs were cloned into pSpCas9(BB)-2A-GFP (PX458, Addgene Plasmid #48138 from Dr. Feng Zhang; ref. 9). Single cells were sorted using flow cytometry, expanded, and clones bearing null alleles were identified by Sanger sequencing and immunoblotting. For gene disruption in cancer cell lines, the gRNAs validated in the Hap1 cells were introduced into LentiCRISPR v2 (Addgene Plasmid #52961 from Dr. Feng Zhang; ref. 10) for lentiviral-mediated delivery. The oligo sequences for guide RNAs are provided in Supplementary Methods.

Haploid genetic screen

Methods for the execution of haploid genetic screening using insertional retroviral mutagenesis and the bioinformatic pipeline to map the distribution of these insertions in the genome have been described in detail previously (8, 11). One hundred million Hap1 cells mutagenized using a gene-trap (GT) bearing retrovirus were treated with doxorubicin (17.5 nmol/L) for 4 days, followed by 1 week of expansion in the absence of doxorubicin prior to harvest. Genome-wide mapping of insertions was performed in a pool of 30 million doxorubicin-resistant cells and compared with insertions mapped in an equal number of unselected, but mutagenized cells. Clonal cell lines carrying a gene trap insertion in a specific location were isolated from the resistant cell pool using a nested PCR strategy.

Western blotting

Antibodies used for immunoblotting are as follows: Rabbit anti-ABCB1 (D3H1Q, 1:1,000) and rabbit anti-TOP2A (D10G9, 1:1,000) from Cell Signaling Technologies; rabbit anti-SMARCB1 (A301-087A-T, 1:1,000), goat anti-SMARCA4 (A303-877A-T, 1:1,000), and rabbit anti-ARID1A (A301-041A-T; 1:1,000) from Bethyl Laboratories; Mouse anti-α-tubulin (T6199, 1:10,000) from Sigma-Aldrich. A detailed description of our cell lysis and Western blotting protocol is given in Supplementary Materials and Methods.

Short-term cell viability (MTT) assay

A total of 5,000 cells were plated in each well of 96-well plate, allowed to grow for 24 hours, and then treated with various concentrations of doxorubicin or other anticancer drugs in quadruplicate for 96 hours prior to being subjected to a standard MTT assay.

Long-term growth assay

A total of 10^5 cells were plated in each well of a 6-well plate. After 24 hours, the cells were treated with 17.5 nmol/L or 30 nmol/L doxorubicin for 10 days. After 10 days, the cells were fixed with 4% paraformaldehyde and stained with 0.05% Crystal violet solution for 1 hour.

Statistical analysis

All graphing, curve-fitting, and statistical analysis was performed in SigmaPlot. Error bars denote SD derived from 3 to 4 replicates. Details of statistical analyses, including identity of test used, replicate numbers, and *P* values for relevant comparisons from all figure panels, are given in Supplementary Table S4.

Results

A haploid genetic screen for mediators of doxorubicin sensitivity

We conducted a genetic screen (12) in Hap1 cells (8), a near-haploid human cell line that enables the generation of null alleles in most genes by insertional mutagenesis (11). One hundred million Hap1 cells were mutagenized by infecting them with a retrovirus carrying a GT construct (Supplementary Fig. S1A), and then the entire population was treated with a concentration of doxorubicin (17.5 nmol/L) that approximates levels achieved in patients (1). This regimen killed 99% of the cells (LC_{99}) after 4 days of continuous treatment (Supplementary Fig. S1B). Cells that survived, presumably because they had acquired an inactivating GT insertion in a gene promoting sensitivity to doxorubicin, were pooled, and the genomic location and orientation of GT insertions were determined by deep sequencing as described previously (Supplementary Fig. S1A; ref. 8).

Genes whose inactivation conferred doxorubicin resistance were identified using two criteria: (i) an enrichment of inactivating insertions (defined as all insertions in exons plus sense insertions in introns) in the selected population compared with the unselected population and (ii) a bias toward sense insertions over antisense insertions in introns in the selected population (Supplementary Table S1 and Supplementary Fig. S1C; ref. 13). A volcano plot based on these two parameters (Fig. 1A) identified two well-established regulators of doxorubicin resistance, *ABCB1* and *TOP2A*, multiple subunits of the SWI/SNF (also known as the SMARC or BAF) nucleosome remodeling complex (14, 15), and multiple subunits of the histone acetylating STAGA complex (16, 17). A total of 35 genes exceeded our FDR-corrected *P* value threshold of 0.01 (Supplementary Table S1; full results are provided in Supplementary Table S3).

The top two hits in our screen were *TOP2A* and *ABCB1*, genes implicated in the leading causes of doxorubicin resistance. GT insertions in *TOP2A* were mostly found in a sense orientation and thus predicted to interrupt transcription. Paradoxically, GT insertions in *ABCB1* were predominantly in an antisense orientation, such that the splice acceptor element would be incapable of interrupting transcription (Supplementary Fig. S1C and S1D). To understand the molecular basis of resistance caused by the unexpected orientation of GT insertions in *ABCB1*, we isolated a clonal cell line carrying a sense insertion near the start of *TOP2A* ($TOP2A^{GT1}$) and four independent clonal cell lines carrying antisense insertions in *ABCB1* ($ABCB1^{GT1\text{-}4}$; Supplementary Fig. S1E). In both short-term (96-hour) viability assays (Fig. 1B) and long-term (10-day) growth assays (Fig. 1C), all five gene-trapped clones showed substantially increased resistance to doxorubicin. In MTT assays, the 50% lethal concentration (LC_{50}), defined as the doxorubicin concentration at which cell viability was reduced by 50% compared with an untreated population, was increased by 4- to 6-fold compared with the parental wild-type (WT) Hap1 cells (Fig. 1B). Analysis of *TOP2A* and *ABCB1* RNA and protein levels in these clonal cell lines revealed the causes of resistance (Fig. 1D). The sense GT insertions significantly reduced TOP2A protein levels, whereas the antisense GT insertions caused a dramatic increase in ABCB1 protein, both through transcriptional

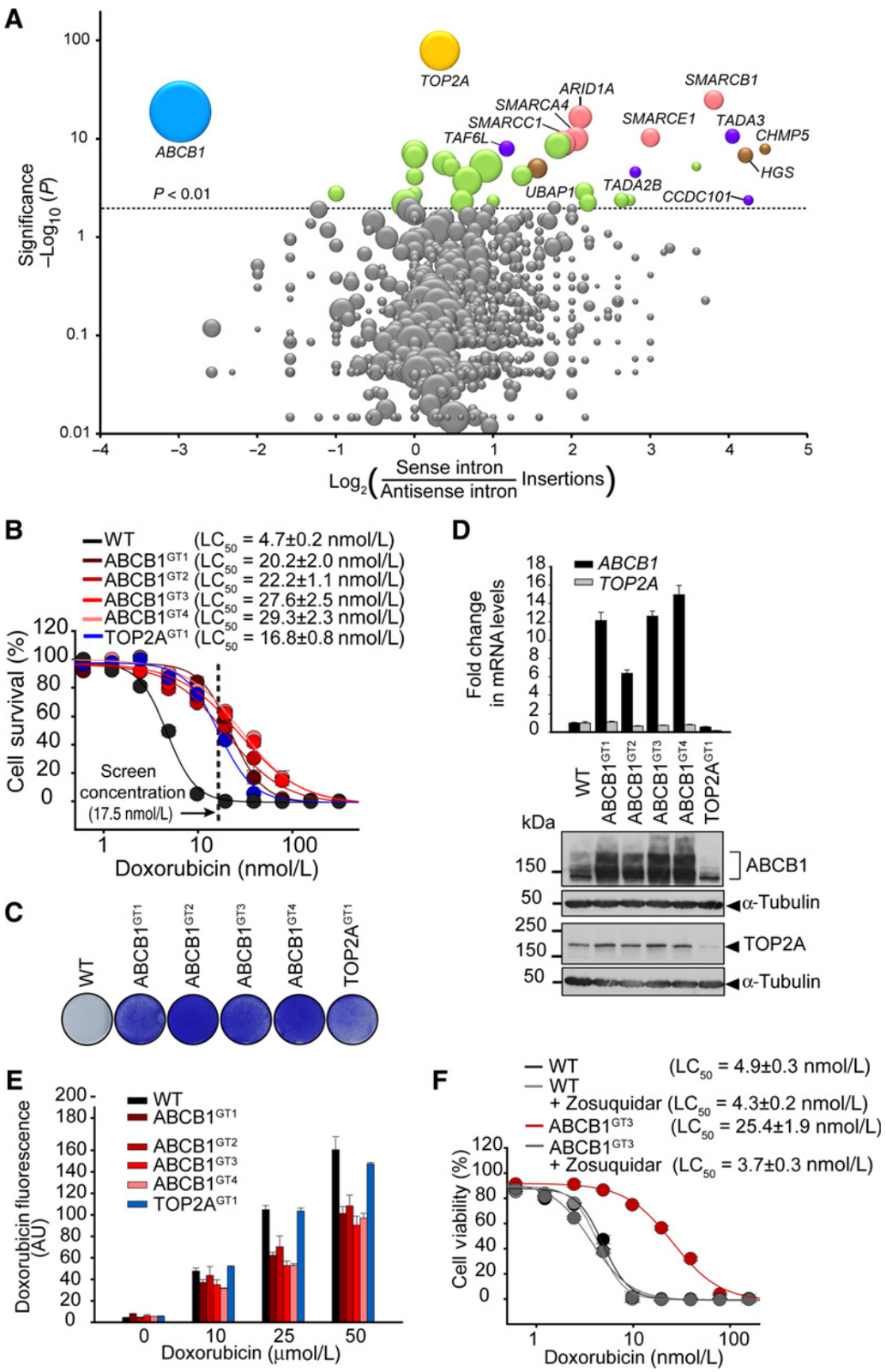
A
ABCB1
TOP2A
ARID1A
SMARCA4
SMARCC1
TAF6L
SMARCE1
SMARCB1
TADA3
CHMP5
HGS
TADA2B
CCDC101
UBAP1
P < 0.01
Significance –Log10 (P)
Log2(Sense intron / Antisense intron Insertions)
B
WT (LC50 = 4.7±0.2 nmol/L)
ABCB1GT1 (LC50 = 20.2±2.0 nmol/L)
ABCB1GT2 (LC50 = 22.2±1.1 nmol/L)
ABCB1GT3 (LC50 = 27.6±2.5 nmol/L)
ABCB1GT4 (LC50 = 29.3±2.3 nmol/L)
TOP2AGT1 (LC50 = 16.8±0.8 nmol/L)
Cell survival (%)
Screen concentration (17.5 nmol/L)
Doxorubicin (nmol/L)
C
WT
ABCB1GT1
ABCB1GT2
ABCB1GT3
ABCB1GT4
TOP2AGT1
D
ABCB1
TOP2A
Fold change in mRNA levels
kDa
150
50
250
150
50
ABCB1
α-Tubulin
TOP2A
α-Tubulin
E
WT
ABCB1GT1
ABCB1GT2
ABCB1GT3
ABCB1GT4
TOP2AGT1
Doxorubicin fluorescence (AU)
Doxorubicin (μmol/L)
F
WT (LC50 = 4.9±0.3 nmol/L)
WT + Zosuquidar (LC50 = 4.3±0.2 nmol/L)
ABCB1GT3 (LC50 = 25.4±1.9 nmol/L)
ABCB1GT3 + Zosuquidar (LC50 = 3.7±0.3 nmol/L)
Cell viability (%)
Doxorubicin (nmol/L)

mechanisms (Fig. 1D). All four cell lines carrying antisense insertions in the *ABCB1* locus accumulated less doxorubicin in a fluorescence-based uptake assay (Fig. 1E). Most importantly, the doxorubicin-resistant phenotype of ABCB1^{GT3} cells could be reversed by Zosuquidar, a potent and specific ABCB1 inhibitor (Fig. 1F; ref. 18). Reversal of the phenotype by Zosuquidar makes it unlikely that doxorubicin resistance in ABCB1^{GT3} cells was caused by passenger insertions at other loci.

In summary, our screen in Hap1 cells identified two leading causes of doxorubicin resistance, decreased *TOP2A* and increased *ABCB1* expression levels, establishing the physiologic relevance of this system. These results also demonstrate the ability of retroviral GT mutagens to generate both hypomorphic and gain-of-function alleles in haploid cells, highlighting their potential to uncover a wider range of genes (including essential genes like *TOP2A*) compared with strict loss-of-function screens.

Proteins that regulate chromatin structure can influence sensitivity to doxorubicin

To validate the SWI/SNF and STAGA complex subunits identified in our screen (Supplementary Table S1), we introduced CRISPR/Cas9-mediated frameshift mutations into *SMARCB1*, *SMARCA4*, *ARID1A*, and *TADA3* using two different guide RNAs (gRNAs) targeting each gene (refs. 9, 19; Supplementary Table S2). Clonal cell lines carrying mutations were isolated and are hereafter denoted as "CR1" or "CR2" following the gene name. We confirmed depletion of SMARCB1, SMARCA4, and ARID1A by immunoblotting (Fig. 2A). As expected, protein levels of some of the SWI/SNF complex subunits were dependent on each other—loss of SMARCB1 led to a decline in ARID1A protein levels and vice versa.

Depletion of SMARCB1, ARID1A, and TADA3 increased resistance to doxorubicin in both short-term MTT assays (Fig. 2B) and long-term growth assays (Fig. 2C). Depletion of SMARCB1 gave the strongest phenotype, leading to a 4-fold increase in the LC_{50} of doxorubicin (Fig. 2B). The loss of SMARCA4 did not significantly change the doxorubicin LC_{50} in MTT assays. However, in longer-term growth assays, SMARCA4^{CR} cells had a growth advantage in the presence of doxorubicin (Fig. 2C), which explains the enrichment of retroviral insertions in *SMARCA4* seen in the screen.

Loss of SMARCB1, but not SMARCA4, increases the expression of *ABCB1*

Loss of SMARCB1 caused the largest increase in the LC_{50} of doxorubicin (Fig. 2B). SMARCB1 is a core subunit of the SWI/SNF complex and a potent tumor suppressor lost in the majority of malignant rhabdoid tumors (MRT; refs. 20–25). SMARCA4 is one of the two alternative ATPase subunits required for the energy-dependent nucleosome remodeling activity of the complex, the other being SMARCA2 (or BRM; ref. 15). Given that both SMARCB1 and SMARCA4 were identified in the screen and that both proteins are core subunits of the SWI/SNF complex, we expected that loss of either would regulate doxorubicin sensitivity by the same mechanism.

We compared the transcriptional profile of WT Hap1 cells with that of their isogenic counterparts lacking either SMARCB1 or SMARCA4 (Fig. 3 and Supplementary Table S5). Though both proteins are part of the same complex, there were striking differences in the genes upregulated by the loss of each protein (Fig. 3). Expression of the most highly upregulated genes in the SMARCB1^{CR} cells compared with WT cells was only minimally altered in SMARCA4^{CR} cells ("CR" following the gene name denotes both "CR1 and CR2"). There was more overlap between the SMARCA4^{CR} and SMARCB1^{CR} expression profiles looking at downregulated genes (Fig. 3A and B). *ABCB1* was the 12th most highly upregulated gene (5.8-fold) in SMARCB1^{CR} cells compared with WT cells (Fig. 3B and Supplementary Table S5). Conversely, *ABCB1* mRNA was 1.7-fold reduced in SMARCA4^{CR} cells compared with WT cells. This suggested that increased ABCB1 levels could cause doxorubicin resistance in SMARCB1^{CR} cells, but that the mechanism whereby *SMARCA4* loss confers doxorubicin resistance was most likely a different one. Among a panel of ABC transporters that have been implicated in doxorubicin resistance, the loss of SMARCB1 also led to the transcriptional upregulation of ABCG2 (Supplementary Fig. S5C); however, absolute mRNA levels of *ABCG2* (even after induction) were much lower than those of *ABCB1* in HAP1 cells.

We measured levels of *ABCB1* mRNA by qRT-PCR and protein by immunoblotting (Fig. 4A) in cell lines lacking individual SWI/SNF components. In agreement with the RNAseq data, *ABCB1* mRNA was upregulated in two independent cell lines (SMARCB1^{CR1} and SMARCB1^{CR2}), and this change was translated into increased ABCB1 protein levels. In contrast, SMARCA4 loss resulted in reduced ABCB1 protein levels, supporting opposing roles of these two core SWI/SNF subunits in *ABCB1* gene regulation. Thus, *SMARCA4* must confer doxorubicin resistance independently of *ABCB1* regulation; however, we did not further pursue this alternative mechanism because of the subtle effects of *SMARCA4* loss on the growth of Hap1 cells in our assays (Fig. 2B and C).

When epitope-tagged SMARCB1-3xHA was stably reintroduced into either SMARCB1^{CR1} or SMARCB1^{CR2} cells, *ABCB1* expression

Figure 1.

A forward genetic screen in human haploid cells for mediators of doxorubicin sensitivity. **A,** volcano plot depicting the results of the screen. Each circle represents a gene, with the diameter scaled according to the number of independent retroviral insertions, plotted based on the *P* value for enrichment of insertions in the doxorubicin-selected population over the control population (*y*-axis) and the bias toward inactivating intronic insertions (*x*-axis). Genes with a FDR-corrected *P* value smaller than 0.01 are colored. Pink, SWI/SNF complex genes; violet, STAGA complex genes; brown, MVB (multivesicular body) trafficking genes; green, other significant genes. Intron-less genes were assigned a sense/antisense insertion ratio (*x*-axis) of 1. The full set of significant genes ($P < 0.01$) with enumeration of insertions is provided in Supplementary Table S1, and the entire dataset for the screen is provided in Supplementary Table S3. **B,** an MTT assay (96 hours) was used to determine the LC_{50} for doxorubicin in cell lines carrying independent gene-trap (GT) insertions in *ABCB1* or *TOP2A*. **C,** crystal violet staining was used to assess cell growth after 10 days (d) of exposure to 17.5 nmol/L doxorubicin. **D,** *ABCB1* and *TOP2A* mRNA (top) and protein levels (bottom) in the indicated GT clones, measured by qRT-PCR and immunoblotting, respectively. Tubulin is shown as a loading control for each of the two separate blots. **E,** doxorubicin accumulation in the indicated cell lines measured by the intrinsic fluorescence of doxorubicin after exposure of cells to various concentrations of the drug for 2 hours. **F,** sensitivity of WT cells or cells with an antisense insertion at the *ABCB1* locus to doxorubicin in the absence or presence of Zosuquidar (100 nmol/L). Error bars, which in many cases are smaller than the diameter of the circles used to denote the mean value, represent the SD ($n = 4$ for **B** and **F** and $n = 3$ for **D** and **E**); *P* values for relevant comparisons are shown in Supplementary Table S4.

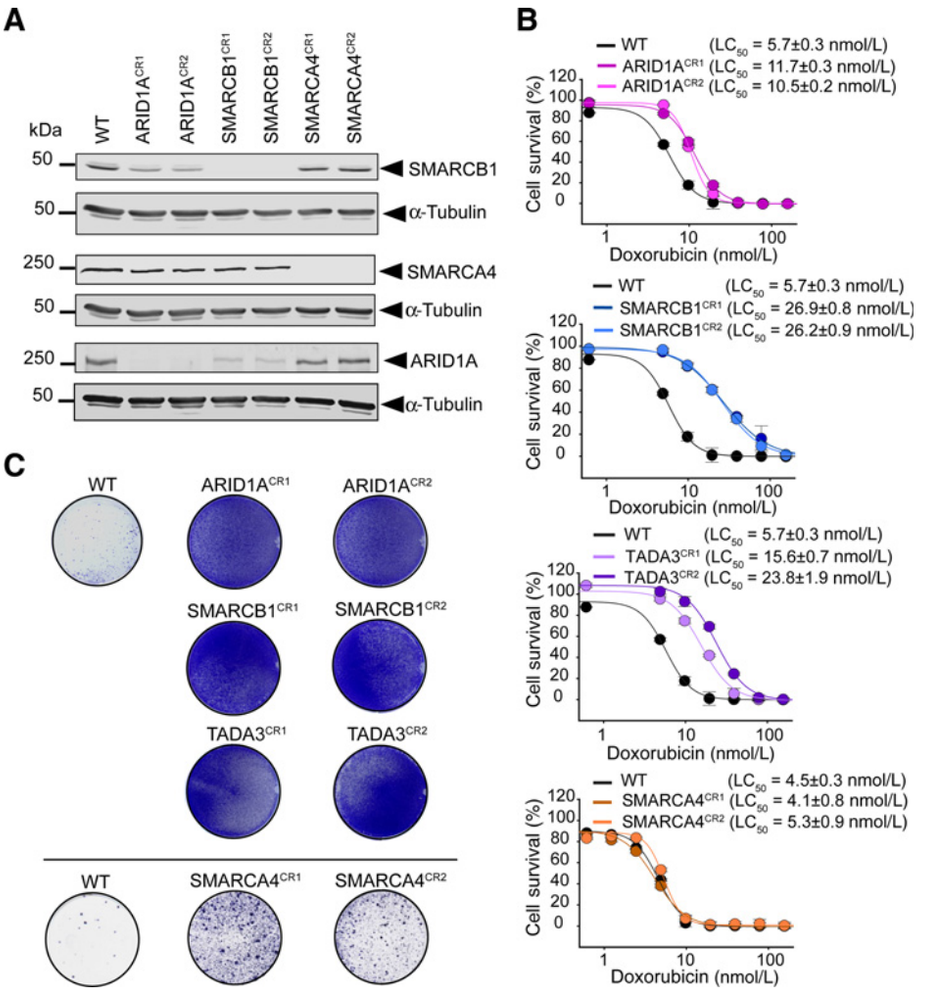

Figure 2.
Disrupting genes that encode components of the SWI/SNF and STAGA chromatin regulatory complexes confers resistance to doxorubicin. **A,** immunoblot showing protein levels of SMARCB1, SMARCA4, and ARID1A in clonal cell lines carrying CRISPR/Cas9-mediated frameshift mutations in the indicated genes. Each gene was targeted with two different guide RNAs (CR1 and CR2; see Supplementary Table S2). Doxorubicin sensitivity in each cell line was determined by MTT assays (96 hours; **B**) or by crystal violet staining after 10 days of exposure to 17.5 nmol/L doxorubicin (**C**).

significantly declined and approached the level of WT cells (Fig. 4B). Importantly, these rescued cells were resensitized to doxorubicin in both short-term (Fig. 4C) and long-term (Fig. 4D) growth assays. This experiment established that the changes in *ABCB1* levels and doxorubicin sensitivity measured in SMARCB1^{CR1} and SMARCB1^{CR2} cell lines were indeed caused by the loss of SMARCB1, rather than by cryptic mutations.

We correlated expression levels of *SMARCB1* and *ABCB1* across 12 human cancers from The Cancer Genome Atlas (TGCA) portal (Supplementary Fig. S2). In ten of twelve cancers, a significant negative correlation was observed between the expression of these two genes, with a Pearson coefficient of linear correlation around −0.2. *ABCB1* mRNA levels were consistently higher among tumors in the bottom quartile of *SMARCB1* expression compared with those in the top quartile. This correlative data are consistent with the negative effect of SMARCB1 on ABCB1 expression seen in Hap1 cells and suggest this regulatory relationship may be relevant in some human cancers. Across several of these cancers, the expression of SMARCB1 was also negatively correlated with a gene-expression signature associated (26) with resistance to doxorubicin (Supplementary Fig. S3).

To provide more direct evidence, SMARCB1 was depleted in five human cancer cell lines infected with lentivirus-based CRISPR/Cas9 (LentiCR) constructs carrying gRNAs validated in Hap1 cells (Supplementary Fig. S4A). In each case, *ABCB1* mRNA was significantly upregulated, ranging from approximately 2-fold in PC3 cells to approximately 17.5-fold in NCI-H1650 cells (Fig. 4E). Conversely, overexpression of SMARCB1-3xHA in the SNU-349 renal cancer cell line, chosen because it expresses high levels of *ABCB1*, led to downregulation of ABCB1 protein (Fig. 4F). Thus, both gain and loss of SMARCB1 function have corresponding opposing effects on *ABCB1* expression in cancer cell lines, consistent with the analysis in Hap1 cells (Fig. 4B) and the correlative observations from TCGA data (Supplementary Figs. S2 and S3).

Doxorubicin resistance in cells lacking SMARCB1 can be reversed by the pharmacologic or genetic ablation of *ABCB1*

SMARCB1 has been implicated in diverse genomic processes, including control of developmental (25) and lineage-specific gene expression (27), nucleosome positioning at promoters (28), and TOP2A recruitment (5), all mechanisms that could contribute to altered sensitivity to doxorubicin. To test whether *ABCB1* overexpression was the cause of doxorubicin resistance in cell lines lacking SWI/SNF subunits, we measured doxorubicin sensitivity in the presence of Zosuquidar. Zosuquidar neutralized the effect of SMARCB1 loss almost completely—the doxorubicin LC_{50} in SMARCB1^{CR1} cells treated with Zosuquidar was reduced

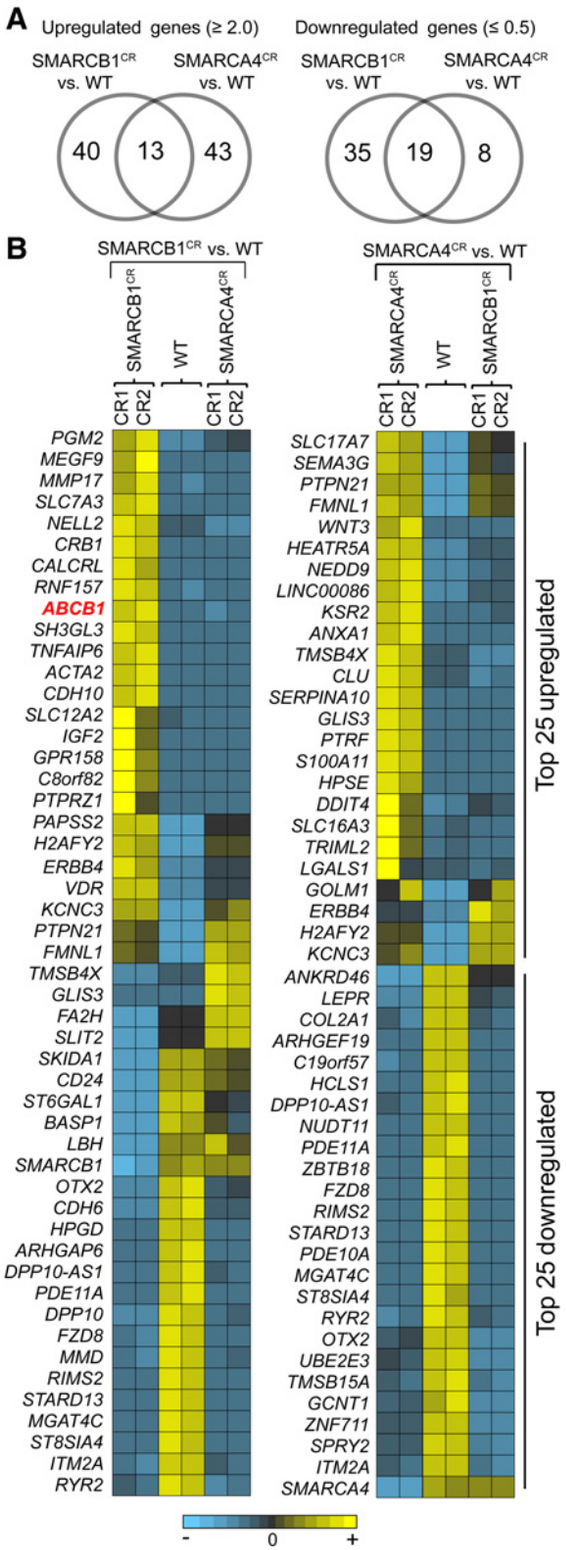

Figure 3.

Gene expression changes in Hap1 cells lacking SMARCB1 or SMARCA4. **A,** Venn diagram showing the number of genes whose expression is increased (left) or decreased (right) in cells lacking SMARCB1 or SMARCA4 compared with WT Hap1. **B,** heatmaps showing relative expression levels across all three cell types for the 25 most up- and downregulated genes in SMARCB1^{CR} compared with WT cells (left) and in SMARCA4^{CR} compared with WT cells (right). Genes are arranged based on hierarchical clustering. Biological replicates for the SMARCB1- and SMARCA4-null cell lines represent two independent clonal cell lines generated by CRISPR methods using two different guide RNAs (CR1 and CR2, see Supplementary Table S2). Replicates for the WT RNAseq data were generated from two different passages of Hap1 cells. Only genes that passed a FDR-corrected *P* value of <0.001 for the indicated comparison and were represented by >1,000 total reads were included in the analyses. The full RNAseq dataset is given in Supplementary Table S5.

by 4-fold, nearly down to that measured in WT cells (Fig. 5A). A similar effect was seen in ARID1A^{CR1} cells (Fig. 5A).

Because small molecules can have off-target effects, we probed the epistatic relationship between *SMARCB1* and *ABCB1* with respect to doxorubicin resistance through an independent genetic approach. We knocked out both *SMARCB1* and *ABCB1* in two independent cell lines (ABCB1$^{CR1.1}$;SMARCB1$^{CR2.1}$ and ABCB1$^{CR1.1}$;SMARCB1$^{CR2.2}$) and compared their doxorubicin sensitivity with that of the corresponding single knock-out cell lines (Fig. 5B). In both short-term (Fig. 5C) and long-term (Fig. 5D) growth assays, *ABCB1* was epistatic to *SMARCB1*—the doxorubicin sensitivity of cells lacking both ABCB1 and SMARCB1 was very similar to that of WT cells or cells lacking only ABCB1, but much greater than that of cells lacking SMARCB1 alone. This result places *ABCB1* downstream of *SMARCB1* and indicates that doxorubicin resistance in cells devoid of SMARCB1 is mediated by ABCB1.

Our results are at odds with a prevailing model (6) in the field that doxorubicin resistance in cells lacking SMARCB1 is due to impaired recruitment of TOP2A to chromatin, a previously described activity of the SWI/SNF complex (5), and a consequent reduction in doxorubicin-mediated DNA damage. Because our analysis was performed in exactly the same Hap1 cell line, it was essential to experimentally address the fundamental differences between our studies.

While both studies used Hap1 cells, the doxorubicin treatment regimens were quite different. We exposed cells continuously to low nanomolar doses of doxorubicin (0–100 nmol/L), comparable with the steady-state concentrations attained by all dosage regimens used in patients (1), whereas the other study treated cells with a two-hour pulse of micromolar concentrations of doxorubicin, presumably to mimic the high peak doxorubicin concentrations achieved by bolus dosing regimens. To determine whether different resistance mechanisms may operate under these two regimes, we exposed WT, SMARCB1^{CR2}, ABCB1$^{CR1.1}$, and ABCB1$^{CR1.1}$;SMARCB1^{CR2} cells to precisely the same doxorubicin treatment protocol described in the other study (6)—a two-hour pulse of 0, 0.25, 0.5, or 1 μmol/L doxorubicin followed by a 10-day growth assay. In agreement with their results, loss of SMARCB1 alone increased resistance to doxorubicin (Fig. 5E and Supplementary Fig. S4B). However, this effect could be reversed by the depletion of ABCB1: the doxorubicin sensitivity of ABCB1$^{CR1.1}$;SMARCB1^{CR2} cells was comparable with that of ABCB1$^{CR1.1}$ cells and significantly higher than that of SMARCB1^{CR2} cells (Fig. 5E and Supplementary Fig. S4B). Again, *ABCB1* was epistatic to *SMARCB1*, supporting a mechanism for doxorubicin resistance in cells lacking SMARCB1 that depends on ABCB1. The identical doxorubicin sensitivity of ABCB1$^{CR1.1}$ and ABCB1$^{CR1.1}$;SMARCB1^{CR2} cells discounts an additional or alternative role for SMARCB1, such as the proposed effects on DNA damage.

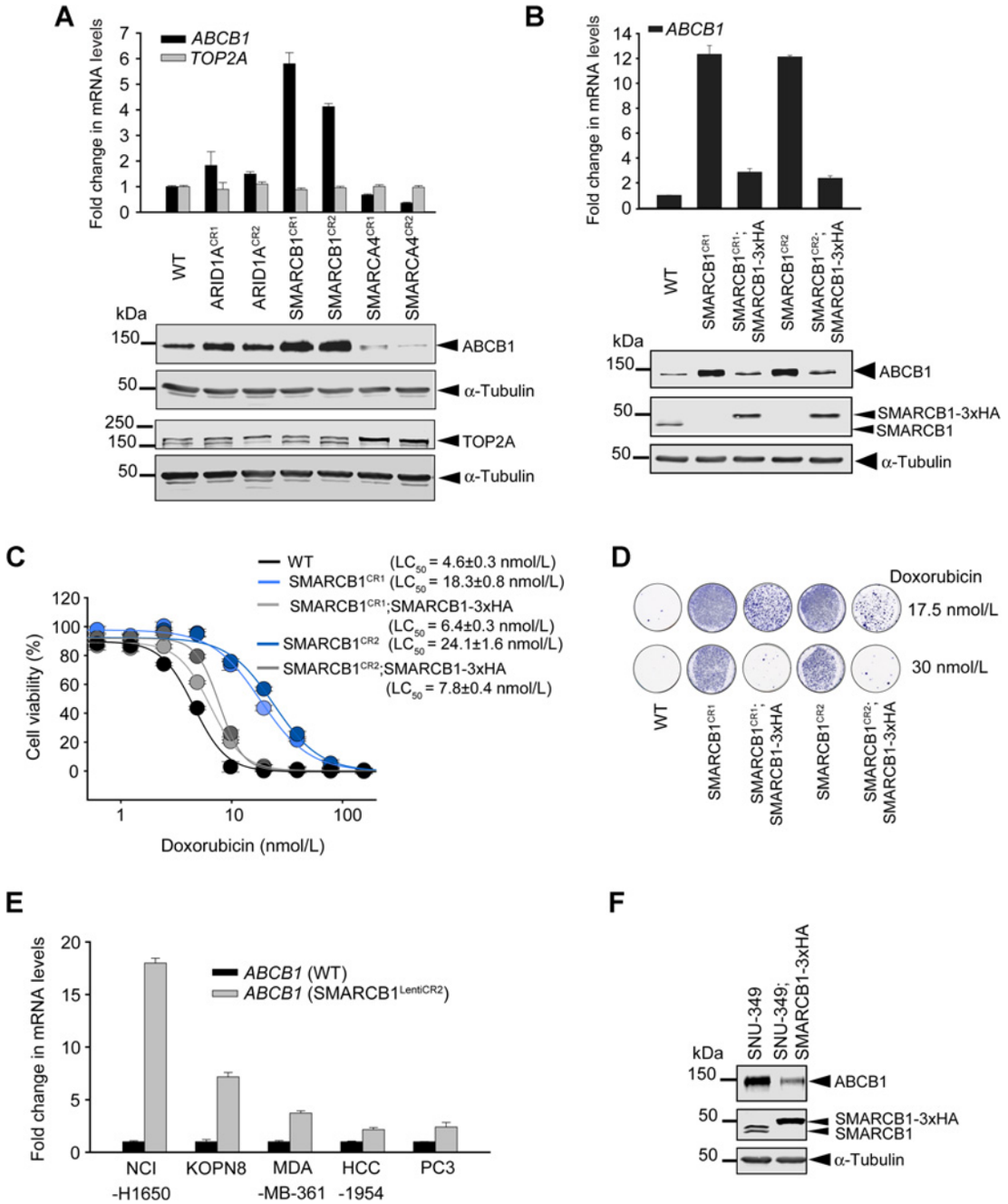

Figure 4.

SMARCB1 disruption increases expression of *ABCB1* in Hap1 cells. **A,** *ABCB1* and *TOP2A* mRNA (top) and protein levels (bottom) in the indicated cell lines, measured by qRT-PCR and immunoblotting, respectively. **B,** re-expression of SMARCB1 (epitope-tagged with 3xHA) in two cell lines (CR1 and CR2) lacking endogenous SMARCB1 leads to a decrease in both *ABCB1* mRNA (top) and protein (bottom). Both cell lines expressing 3xHA-SMARCB1 show increased sensitivity to doxorubicin in 96-hour MTT assays (**C**) and 10-day growth assays (**D**). **E,** *ABCB1* mRNA was measured by qRT-PCR in several cancer cell lines infected with a control lentivirus or a lentivirus carrying a validated gRNA (Lenti^{CR2}) against SMARCB1. Levels of SMARCB1 were assessed by immunoblotting, as shown in Supplementary Fig. S4A. **F,** ABCB1 protein levels were measured by immunoblotting in SNU-349 cells stably overexpressing epitope-tagged SMARCB1. Error bars, SD ($n = 3$ in **A, B,** and **E**; $n = 4$ in **C**); *P* values for relevant comparisons are shown in Supplementary Table S4.

These two mechanisms of resistance to doxorubicin, ABCB1 overproduction, or reduced TOP2A recruitment predict very different therapeutic consequences. Our mechanism, *ABCB1* overexpression, predicts that cells lacking SMARCB1 will be resistant, not only to TOP2A-targeted drugs like doxorubicin, but also to other classes of chemotherapeutics that are substrates of ABCB1,

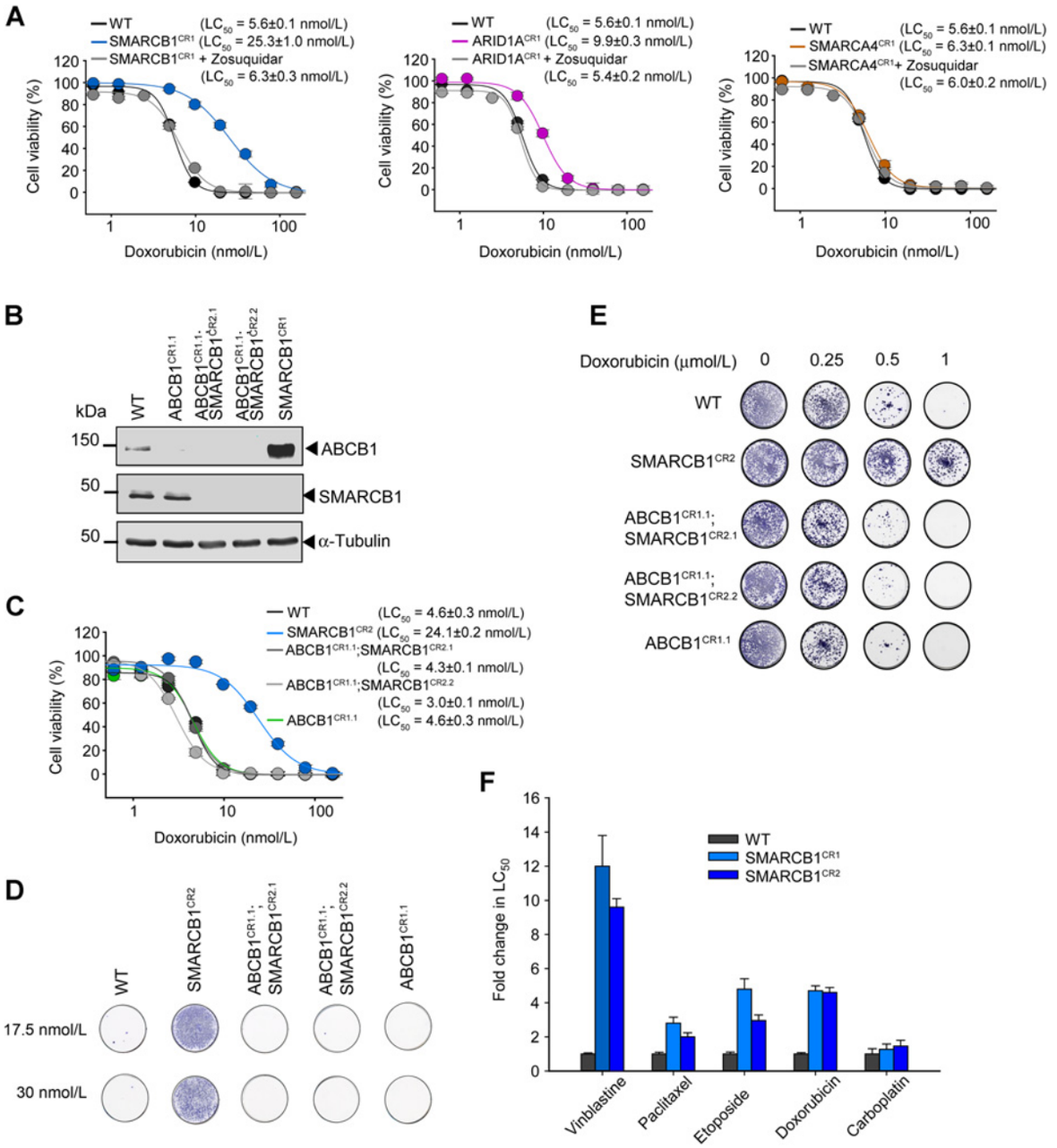

Figure 5.

ABCB1 is required for doxorubicin resistance in Hap1 cells lacking SMARCB1. **A,** doxorubicin LC_{50} was measured using an MTT assay (96 hours) in cell lines lacking SMARCB1 (left), ARID1A (middle), and SMARCA4 (right) in the absence or presence of Zosuquidar (100 nmol/L). **B,** immunoblotting was used to compare the protein levels of ABCB1 in $SMARCB1^{CR2}$ cells, $ABCB1^{CR1}$ cells, and in two independent clonal cell lines carrying frameshift mutations in both *SMARCB1* and *ABCB1*. Doxorubicin sensitivity in each of these single and double mutant cell lines was measured using a 96-hour MTT assay (**C**) or a 10-day growth assay (**D**). **E,** single and double mutant cell lines were treated with a transient 2-hour pulse of doxorubicin, followed by drug removal, and growth for 10 days. Crystal violet staining used to assess cell growth after this treatment regimen is shown in **E** and quantified in Supplementary Fig. S4B. Error bars, SD ($n = 4$ in **A** and **C**). **F,** fold increases in the LC_{50} for various drugs in two cell lines carrying independent frameshift mutations in SMARCB1. Vinblastine and paclitaxel are microtubule-targeted ABCB1 substrates, etoposide and doxorubicin are TOP2A-targeted ABCB1 substrates, and carboplatin is not considered an ABCB1 substrate. Drug resistance induced by SMARCB1 loss can be reversed by adding the ABCB1-inhibitor Zosuquidar (Supplementary Fig. S4C).

such as the microtubule-targeted taxanes or vinca alkaloids. The alternative mechanism predicts that resistance should be restricted to TOP2A-targeted drugs; sensitivity to microtubule-targeted agents should be unaffected. Indeed, two independent cell lines lacking SMARCB1 show increased resistance to both paclitaxel and vinblastine, consistent with a multidrug resistant (MDR)

phenotype conferred by ABCB1 overexpression (Fig. 5F and Supplementary Fig. S4C).

The myriad lines of experimental data presented above prove that doxorubicin resistance in cells lacking SMARCB1 is due to increased expression of the drug efflux pump ABCB1. The diminished DNA damage measured in the previous study (6) when SMARCB1 is lost is likely to be a secondary consequence of the reduced intracellular accumulation of doxorubicin and the other TOP2A poisons used in that study (all of which are ABCB1 substrates). Indeed, Hap1 cells lacking SMARCB1 accumulated lower levels of two structurally distinct ABCB1 substrates, doxorubicin itself, and the nontoxic Rhodamine-123 (ref. 29; Supplementary Fig. S4D and S4E).

Doxorubicin resistance in cells lacking SMARCB1 depends on SMARCA4

Given that SMARCB1 and SMARCA4 are two core components of the same protein complex, how can they have opposing effects on *ABCB1* gene expression (Fig. 4A)? To understand their epistatic relationship, we engineered a double mutant Hap1 cell line ($SMARCB1^{CR1}$;$SMARCA4^{CR2}$) lacking expression of both SMARCB1 and SMARCA4. The elevated ABCB1 protein and mRNA levels seen in $SMARCB1^{CR1}$ cells were markedly reduced by the additional depletion of SMARCA4, returning to levels approximating those found in WT cells (Fig. 6A). The reduction in ABCB1 observed in $SMARCB1^{CR1}$;$SMARCA4^{CR2}$ cells also led to increased doxorubicin sensitivity in both short-term (Fig. 6B) and long-term (Fig. 6C) growth assays. The low *ABCB1* expression and doxorubicin sensitivity measured in $SMARCB1^{CR1}$;$SMARCA4^{CR2}$ cells resembled the phenotype of $SMARCA4^{CR2}$ cells, consistent with a model in which SMARCA4 function is epistatic to SMARCB1 function.

We tested whether SMARCA4 also functions downstream of SMARCB1 in the lung cancer cell line A549, which does not express endogenous SMARCA4 (Fig. 6D). Loss of SMARCB1 in A549 cells did not alter ABCB1 levels, consistent with the observation from Hap1 cells that *ABCB1* upregulation in this setting depends on the function of SMARCA4. Indeed, the expression of SMARCA4-FLAG in A549 cells lacking SMARCB1 led to the induction of *ABCB1* protein and mRNA (Fig. 6E). These results in Hap1 and A549 cells demonstrate that SMARCA4 is a critical barrier to *ABCB1* expression, and consequently drug sensitivity, when the tumor suppressor SMARCB1 is lost.

Transcriptional profiling of the double mutant $SMARCB1^{CR1}$;$SMARCA4^{CR2}$ cells, compared with the corresponding single mutant cell lines, revealed a larger set of "ABCB1-like" genes whose increased expression when SMARCB1 is lost depends on the continued function of SMARCA4 (Supplementary Fig. S5). More generally, genes could be classified into distinct groups based on whether their expression was modulated by SMARCA4, SMARCB1, or both proteins (Supplementary Fig. S5 and Supplementary Table S6), suggesting that SWI/SNF complexes composed of different combinations of these core subunits can regulate distinct sets of genes.

Discussion

The SWI/SNF complex is a tumor suppressor mutated in up to 20% of human cancers (30–32), comparable with mutation rates for iconic tumor suppressors such as *P53* or *PTEN*. We uncovered a novel mechanism by which SWI/SNF complex subunits can influence the efficacy of cancer drugs—through transcriptional regulation of the major multidrug resistance pump implicated in human cancer, ABCB1. ABCB1 substrates include anthracyclines, used as the selective agent in our haploid screen, but also other classes of commonly used drugs in oncology such as the taxanes, vinca alkaloids, and epipodophyllotoxins (33). The loss of SMARCB1, the SWI/SNF subunit with the greatest impact on doxorubicin sensitivity, leads to transcriptional upregulation of *ABCB1* and resistance to both TOP2A-targeted and microtubule-targeted drugs. Both effects can be completely reversed by the genetic or pharmacologic ablation of ABCB1 (Fig. 5C). Among a panel of ABC transporters that have been implicated in doxorubicin resistance, the loss of SMARCB1 also led to the transcriptional upregulation of *ABCG2* (Supplementary Fig. S5C); however, absolute mRNA levels of *ABCG2* (even after induction) were much lower than those of *ABCB1* in HAP1 cells. While ABCG2 upregulation does not play a major role in HAP1 cells, confirmed by our genetic analysis, it may be important in other tumor contexts. Our results also do not support the model (6) that SMARCB1 loss contributes to doxorubicin resistance by reducing the recruitment of TOP2A to DNA. We speculate that the reduced DNA DSBs observed when SMARCB1 is lost are not due to impaired recruitment of TOP2A to DNA, but rather simply due to reduced intracellular levels of doxorubicin.

Our specific analysis of the *ABCB1* locus (Fig. 6) and a more global analysis of gene expression profiles (Supplementary Fig. S5) suggest a complex interaction between SMARCA4 and SMARCB1 in regulating the activity of the SWI/SNF complex. The most parsimonious model, one in which *ABCB1* is repressed by the SWI/SNF complex, is inconsistent with the observation that depletion of SMARCA4 in SMARCB1-null cells leads to reduction of ABCB1 back to WT levels. Instead, this result points to an activating, gain-of-function role for SWI/SNF complexes in the absence of SMARCB1. The picture that emerges is one in which residual SWI/SNF complexes lacking SMARCB1 have different, and even opposite, functions in transcriptional regulation compared with intact complexes. Indeed, in the context of SMARCB1-loss, SMARCA4 becomes a vulnerability because its loss sensitizes cells to doxorubicin by downregulating ABCB1 transcription (Fig. 6).

Our results are consistent with the emerging view that aberrant SWI/SNF complexes play important pathogenic roles when one subunit is lost (33–37), an unexpected concept that first emerged from the discovery that oncogenesis driven by the loss of SMARCB1 could be prevented by the concomitant loss of SMARCA4 (34). This is analogous to our observation that *ABCB1* overexpression and doxorubicin resistance driven by the loss of SMARCB1 could be reversed by eliminating SMARCA4. As a consequence, strategies being developed to target these pathogenic residual SWI/SNF complexes may also improve sensitivity to chemotherapeutics that are substrates of ABCB1.

While we cannot distinguish whether *ABCB1* is directly or indirectly regulated by SWI/SNF complexes, a simple model (Fig. 6F) consistent with the data postulates two populations of SMARCA4-containing SWI/SNF complexes, those with or without SMARCB1, that have opposing effects on *ABCB1* expression. The former would either have no influence on *ABCB1* expression or could have a repressive role, whereas the latter must have an activating role because additional removal of SMARCA4 reverts the activation of target genes like *ABCB1*. The levels of SMARCB1 could regulate the relative proportion of these complexes.

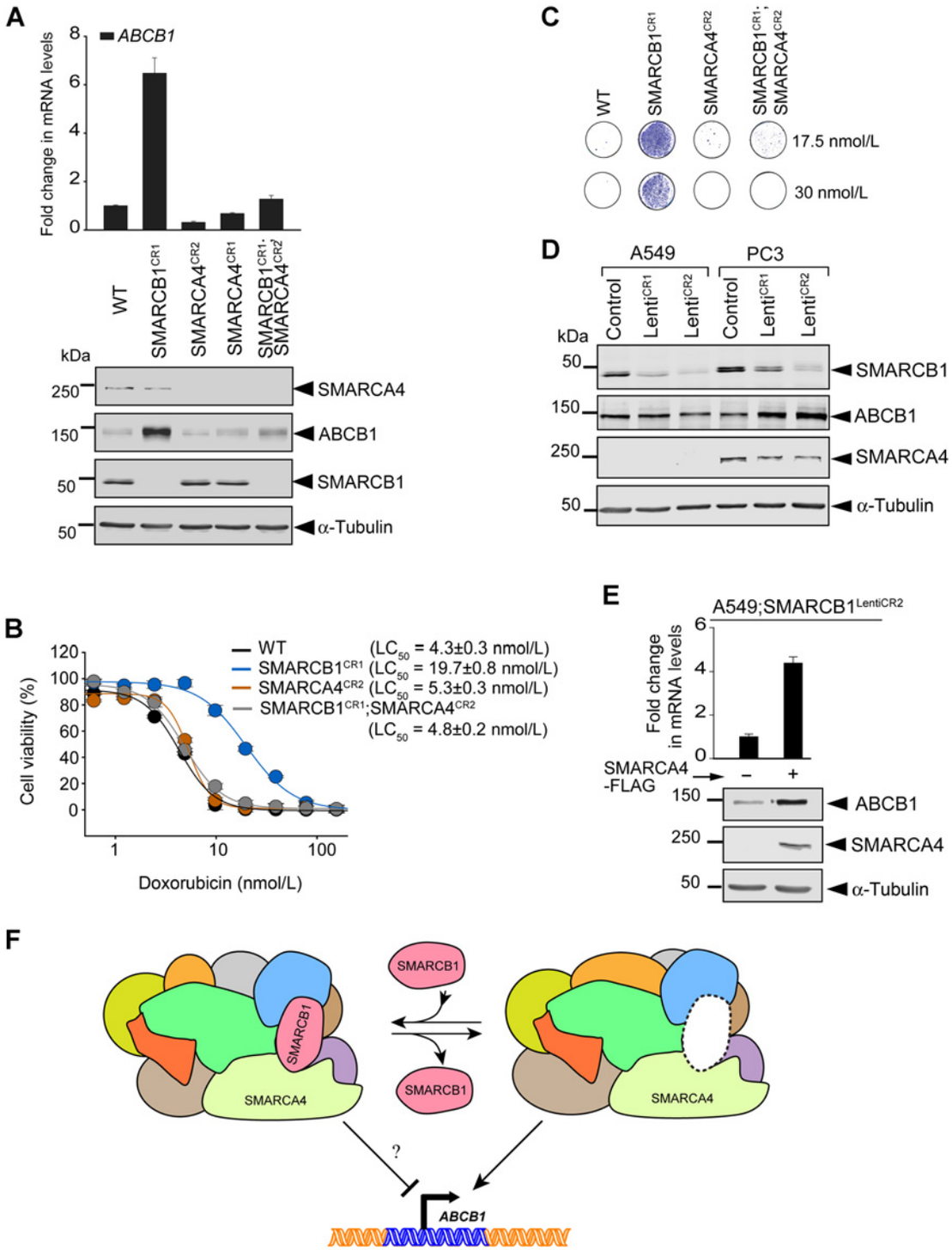

Figure 6.

SMARCA4 is required for elevated *ABCB1* expression in cells lacking SMARCB1. **A,** *ABCB1* mRNA (top) and protein levels (bottom) in clonal cell lines carrying frameshift mutations in *SMARCB1, SMARCA4,* or both genes (SMARCB1^{CR1};SMARCA4^{CR2} cells). Doxorubicin sensitivity in each of these single and double mutant cell lines was measured using a 96-hour MTT assay (**B**) or a 10-day growth assay (**C**). **D,** ABCB1 protein levels were measured to assess the effect of SMARCB1 depletion (using two independent gRNAs, Lenti^{CR1}, and Lenti^{CR2}) in A549 cells, which do not express endogenous SMARCA4, or PC3 cells, which do express endogenous SMARCA4. **E,** *ABCB1* mRNA (top) and protein (bottom) levels were measured in A549 cells depleted of endogenous SMARCB1 (A549; SMARCB1^{LentiCR2} cells) before or after the stable expression of epitope-tagged SMARCA4-FLAG. **F,** a model for the regulation of *ABCB1* by SWI/SNF complexes assembled with or without SMARCB1. See the main text for a description. Error bars, SD ($n = 3$ in **A**; $n = 4$ in **B**).

When SMARCB1 is lost, the activating complexes would predominate and drive expression of *ABCB1* and other target genes subject to similar regulation (Supplementary Fig. S5B). Thus, loss of SMARCB1 would increase the abundance (or activity) of SWI/SNF complexes that drive a gene expression program promoting both oncogenic transformation and drug resistance. More generally, our gene expression data suggest that SWI/SNF complexes that vary in their occupancy by SMARCB1 or SMARCA4 regulate target genes differently, even though both are considered core subunits (Supplementary Fig. S5A). We speculate that levels of these subunits could be used to regulate large sets of genes during development or lineage specification, by controlling the composition or activity of SWI/SNF complexes.

In addition to the SWI/SNF complex, our genome-wide haploid genetic screen in cultured human cells revealed 35 candidate genetic loci (Supplementary Table S1) that may regulate sensitivity to doxorubicin, including several other genes that encode chromatin regulatory proteins. A majority of these genes have not been implicated in resistance to anthracyclines and thus represent an important resource for further investigations into how cells respond to this important class of drugs that remains one of the backbones of current chemotherapy regimens.

Disclosure of Potential Conflicts of Interest

No potential conflicts of interest were disclosed.

Authors' Contributions

Conception and design: R. Dubey, A.M. Lebensohn, Z. Bahrami-Nejad, J.E. Carette, R. Rohatgi

Development of methodology: R. Dubey, A.M. Lebensohn, Z. Bahrami-Nejad, C. Marceau, O. Gevaert, R. Rohatgi

Acquisition of data (provided animals, acquired and managed patients, provided facilities, etc.): R. Dubey, A.M. Lebensohn, C. Marceau, R. Rohatgi

Analysis and interpretation of data (e.g., statistical analysis, biostatistics, computational analysis): R. Dubey, A.M. Lebensohn, M. Champion, O. Gevaert, B.I. Sikic, J.E. Carette, R. Rohatgi

Writing, review, and/or revision of the manuscript: R. Dubey, A.M. Lebensohn, O. Gevaert, B.I. Sikic, R. Rohatgi

Administrative, technical, or material support (i.e., reporting or organizing data, constructing databases): R. Dubey, C. Marceau, R. Rohatgi

Study supervision: R. Dubey, J.E. Carette, R. Rohatgi

Acknowledgments

We are grateful to Bhaven Patel for help with the mapping and analysis of gene trap insertions.

Grant Support

The work was funded by DP2 AI104557 (J.E. Carette), DP2 GM105448 (R. Rohatgi), R01 CA114037 (B.I. Sikic), R01 CA184968 (B.I. Sikic), and start-up funds from the Stanford Cancer Institute (R. Rohatgi). J.E. Carette is a David and Lucile Packard Foundation fellow, and R. Rohatgi is a Josephine Q. Berry Faculty Scholar in Cancer Research at Stanford. R. Dubey was supported by fellowship from the Stanford Dean's Fund and Alex's Lemonade Stand Foundation. A.M. Lebensohn was supported by fellowships from the Stanford Dean's Fund, the Stanford Cancer Biology Training Program, and the Helen Hay Whitney Foundation.

The costs of publication of this article were defrayed in part by the payment of page charges. This article must therefore be hereby marked *advertisement* in accordance with 18 U.S.C. Section 1734 solely to indicate this fact.

Received March 15, 2016; revised June 10, 2016; accepted June 27, 2016; published OnlineFirst August 8, 2016.

References

1. Gewirtz DA. A critical evaluation of the mechanisms of action proposed for the antitumor effects of the anthracycline antibiotics adriamycin and daunorubicin. Biochem Pharmacol 1999;57:727–41.
2. Pommier Y, Leo E, Zhang H, Marchand C. DNA topoisomerases and their poisoning by anticancer and antibacterial drugs. Chem Biol 2010;17:421–33.
3. Kaufmann SH, Karp JE, Jones RJ, Miller CB, Schneider E, Zwelling LA, et al. Topoisomerase II levels and drug sensitivity in adult acute myelogenous leukemia. Blood 1994;83:517–30.
4. Burgess DJ, Doles J, Zender L, Xue W, Ma B, McCombie WR, et al. Topoisomerase levels determine chemotherapy response in vitro and in vivo. Proc Natl Acad Sci U S A 2008;105:9053–8.
5. Dykhuizen EC, Hargreaves DC, Miller EL, Cui K, Korshunov A, Kool M, et al. BAF complexes facilitate decatenation of DNA by topoisomerase IIalpha. Nature 2013;497:624–7.
6. Wijdeven RH, Pang B, van der Zanden SY, Qiao X, Blomen V, Hoogstraat M, et al. Genome-wide identification and characterization of novel factors conferring resistance to topoisomerase II poisons in cancer. Cancer Res 2015;75:4176–87.
7. Juliano RL, Ling V. A surface glycoprotein modulating drug permeability in Chinese hamster ovary cell mutants. Biochim Biophys Acta 1976;455:152–62.
8. Carette JE, Raaben M, Wong AC, Herbert AS, Obernosterer G, Mulherkar N, et al. Ebola virus entry requires the cholesterol transporter Niemann-Pick C1. Nature 2011;477:340–3.
9. Ran FA, Hsu PD, Wright J, Agarwala V, Scott DA, Zhang F. Genome engineering using the CRISPR-Cas9 system. Nat Protoc 2013;8:2281–308.
10. Sanjana NE, Shalem O, Zhang F. Improved vectors and genome-wide libraries for CRISPR screening. Nat Methods 2014;11:783–4.
11. Carette JE, Guimaraes CP, Wuethrich I, Blomen VA, Varadarajan M, Sun C, et al. Global gene disruption in human cells to assign genes to phenotypes by deep sequencing. Nat Biotechnol 2011;29:542–6.
12. Carette JE, Guimaraes CP, Varadarajan M, Park AS, Wuethrich I, Godarova A, et al. Haploid genetic screens in human cells identify host factors used by pathogens. Science 2009;326:1231–5.
13. Blomen VA, Majek P, Jae LT, Bigenzahn JW, Nieuwenhuis J, Staring J, et al. Gene essentiality and synthetic lethality in haploid human cells. Science 2015;350:1092–6.
14. Wang W, Cote J, Xue Y, Zhou S, Khavari PA, Biggar SR, et al. Purification and biochemical heterogeneity of the mammalian SWI-SNF complex. EMBO J 1996;15:5370–82.
15. Phelan ML, Sif S, Narlikar GJ, Kingston RE. Reconstitution of a core chromatin remodeling complex from SWI/SNF subunits. Mol Cell 1999;3:247–53.
16. Martinez E, Palhan VB, Tjernberg A, Lymar ES, Gamper AM, Kundu TK, et al. Human STAGA complex is a chromatin-acetylating transcription coactivator that interacts with pre-mRNA splicing and DNA damage-binding factors in vivo. Mol Cell Biol 2001;21:6782–95.
17. Wang YL, Faiola F, Xu M, Pan S, Martinez E. Human ATAC Is a GCN5/PCAF-containing acetylase complex with a novel NC2-like histone fold module that interacts with the TATA-binding protein. J Biol Chem 2008;283:33808–15.
18. Dantzig AH, Shepard RL, Cao J, Law KL, Ehlhardt WJ, Baughman TM, et al. Reversal of P-glycoprotein-mediated multidrug resistance by a potent cyclopropyldibenzosuberane modulator, LY335979. Cancer Res 1996;56:4171–9.
19. Cong L, Ran FA, Cox D, Lin S, Barretto R, Habib N, et al. Multiplex genome engineering using CRISPR/Cas systems. Science 2013;339:819–23.
20. Biegel JA, Zhou JY, Rorke LB, Stenstrom C, Wainwright LM, Fogelgren B. Germ-line and acquired mutations of INI1 in atypical teratoid and rhabdoid tumors. Cancer Res 1999;59:74–9.
21. Versteege I, Sevenet N, Lange J, Rousseau-Merck MF, Ambros P, Handgretinger R, et al. Truncating mutations of hSNF5/INI1 in aggressive paediatric cancer. Nature 1998;394:203–6.

22. Roberts CWM, Galusha SA, McMenamin ME, Fletcher CDM, Orkin SH. Haploinsufficiency of Snf5 (integrase interactor 1) predisposes to malignant rhabdoid tumors in mice. Proc Natl Acad Sci U S A 2000;97:13796–800.
23. Roberts CWM, Orkin SH. The SWI/SNF complex - chromatin and cancer. Nat Rev Cancer 2004;4:133–42.
24. Wilson BG, Roberts CWM. SWI/SNF nucleosome remodellers and cancer. Nat Rev Cancer 2011;11:481–92.
25. Klochendler-Yeivin A, Fiette L, Barra J, Muchardt C, Babinet C, Yaniv M. The murine SNF5/INI1 chromatin remodeling factor is essential for embryonic development and tumor suppression. EMBO Rep 2000;1:500–6.
26. AbuHammad S, Zihlif M. Gene expression alterations in doxorubicin resistant MCF7 breast cancer cell line. Genomics 2013;101:213–20.
27. Chi TH, Wan M, Zhao K, Taniuchi I, Chen L, Littman DR, et al. Reciprocal regulation of CD4/CD8 expression by SWI/SNF-like BAF complexes. Nature 2002;418:195–9.
28. Tolstorukov MY, Sansam CG, Lu P, Koellhoffer EC, Helming KC, Alver BH, et al. Swi/Snf chromatin remodeling/tumor suppressor complex establishes nucleosome occupancy at target promoters. Proc Natl Acad Sci U S A 2013;110:10165–70.
29. Minderman H, Vanhoefer U, Toth K, Yin MB, Minderman MD, Wrzosek C, et al. DiOC2(3) is not a substrate for multidrug resistance protein (MRP)-mediated drug efflux. Cytometry 1996;25:14–20.
30. Kadoch C, Hargreaves DC, Hodges C, Elias L, Ho L, Ranish J, et al. Proteomic and bioinformatic analysis of mammalian SWI/SNF complexes identifies extensive roles in human malignancy. Nat Genet 2013;45:592–601.
31. Shain AH, Pollack JR. The spectrum of SWI/SNF mutations, ubiquitous in human cancers. PLoS One 2013;8:e55119.
32. Masliah-Planchon J, Bieche I, Guinebretiere JM, Bourdeaut F, Delattre O. SWI/SNF chromatin remodeling and human malignancies. Annu Rev Pathol 2015;10:145–71.
33. Chen KG, Sikic BI. Molecular pathways: Regulation and therapeutic implications of multidrug resistance. Clin Cancer Res 2012;18:1863–9.
34. Wang X, Sansam CG, Thom CS, Metzger D, Evans JA, Nguyen PTL, et al. Oncogenesis caused by loss of the SNF5 tumor suppressor is dependent on activity of BRG1, the ATPase of the SWI/SNF chromatin remodeling complex. Cancer Res 2009;69:8094–101.
35. Helming KC, Wang X, Wilson BG, Vazquez F, Haswell JR, Manchester HE, et al. ARID1B is a specific vulnerability in ARID1A-mutant cancers. Nat Med 2014;20:251–4.
36. Helming KC, Wang X, Roberts CW. Vulnerabilities of mutant SWI/SNF complexes in cancer. Cancer Cell 2014;26:309–17.
37. Wilson BG, Helming KC, Wang X, Kim Y, Vazquez F, Jagani Z, et al. Residual complexes containing SMARCA2 (BRM) underlie the oncogenic drive of SMARCA4 (BRG1) mutation. Mol Cell Biol 2014;34:1136–44.

Supplementary Figure 1

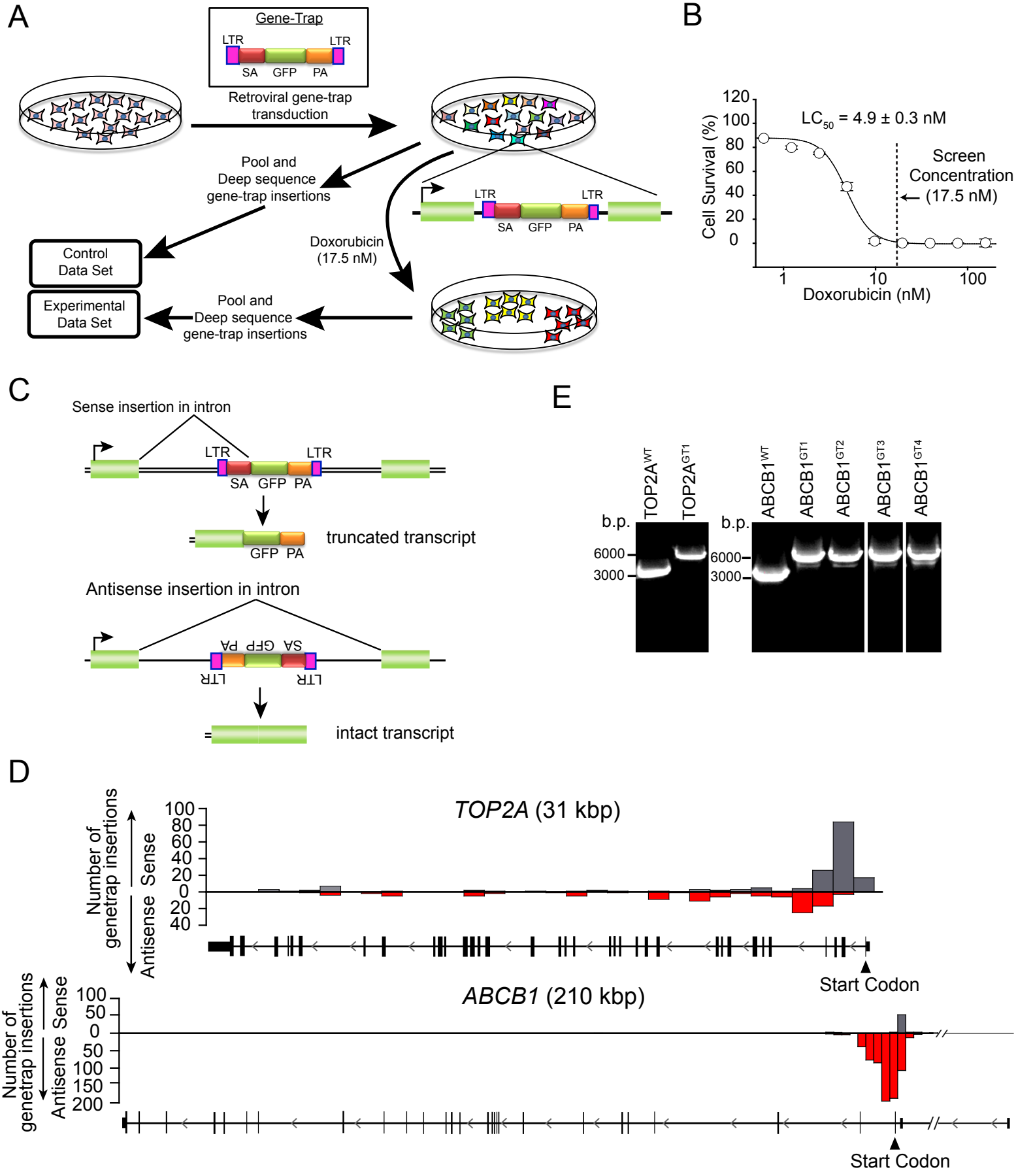

Supplementary Figure 1. Overview of the screening strategy in haploid cells. (**A**) One-hundred million cells were mutagenized by infection with a retrovirus carrying a Gene-Trap (GT) construct. The genomic locations of GT integrations in pooled populations were determined by deep sequencing either before Dox treatment (control set) or after treatment with 17.5 nM Dox (experimental data set). Genes that promote Dox sensitivity are expected to contain a greater number of inactivating insertions in the Dox selected population compared to the unselected population. (**B**) The viability of Hap1 cells as a function of increasing Dox concentration was measured using an MTT assay after 96 hrs. The LC_{50}, the concentration at which viability was reduced by 50% compared to untreated cells, was determined using a non-linear curve fit to the dose-response data. Error bars denote S.D. (*n*=4). (**C**) Two fates of integrations in introns of genes. Sense integrations (top) lead to a splicing event between the splice acceptor (SA) in the GT with the splice donor (SD) of the preceding exon, leading to truncation of the transcript by the poly-adenylation (pA) sequence in the GT cassette. In the case of anti-sense integrations (bottom), the SA in the GT is inverted with respect to gene transcription and hence cannot participate in splicing. In this case the GT cassette is spliced out and cannot trigger truncation of the transcript. Abbreviations are LTR (long terminal repeat), SA (splice acceptor), GFP (green fluorescent protein), pA (poly-adenylation sequence). (**D**) The position and orientation of gene-trap insertions relative to the direction of gene transcription (right to left for both *TOP2A* and *ABCB1*). Each gene was divided into consecutive bins of 1000 base pairs (bp), and the bar graph represents the number of sense (grey) and anti-sense (red) insertions relative to the direction of transcription. (**E**) Genomic PCR with primers flanking retroviral integration sites reveals the insertions at *TOP2A* or *ABCB1* loci for each mutant cell line used in this study and demonstrates both clonality and lack of contamination with cells containing wild-type alleles. The bands just above the 3000 bp marker are at the size for the predicted amplicon from the WT locus, while the bands around 6000 bp marker contain the 2600 bp retroviral insert. The precise genomic location of each retroviral insertion was determined by sequencing with a primer targeted to one end of the gene-trap.

Supplementary Figure 2

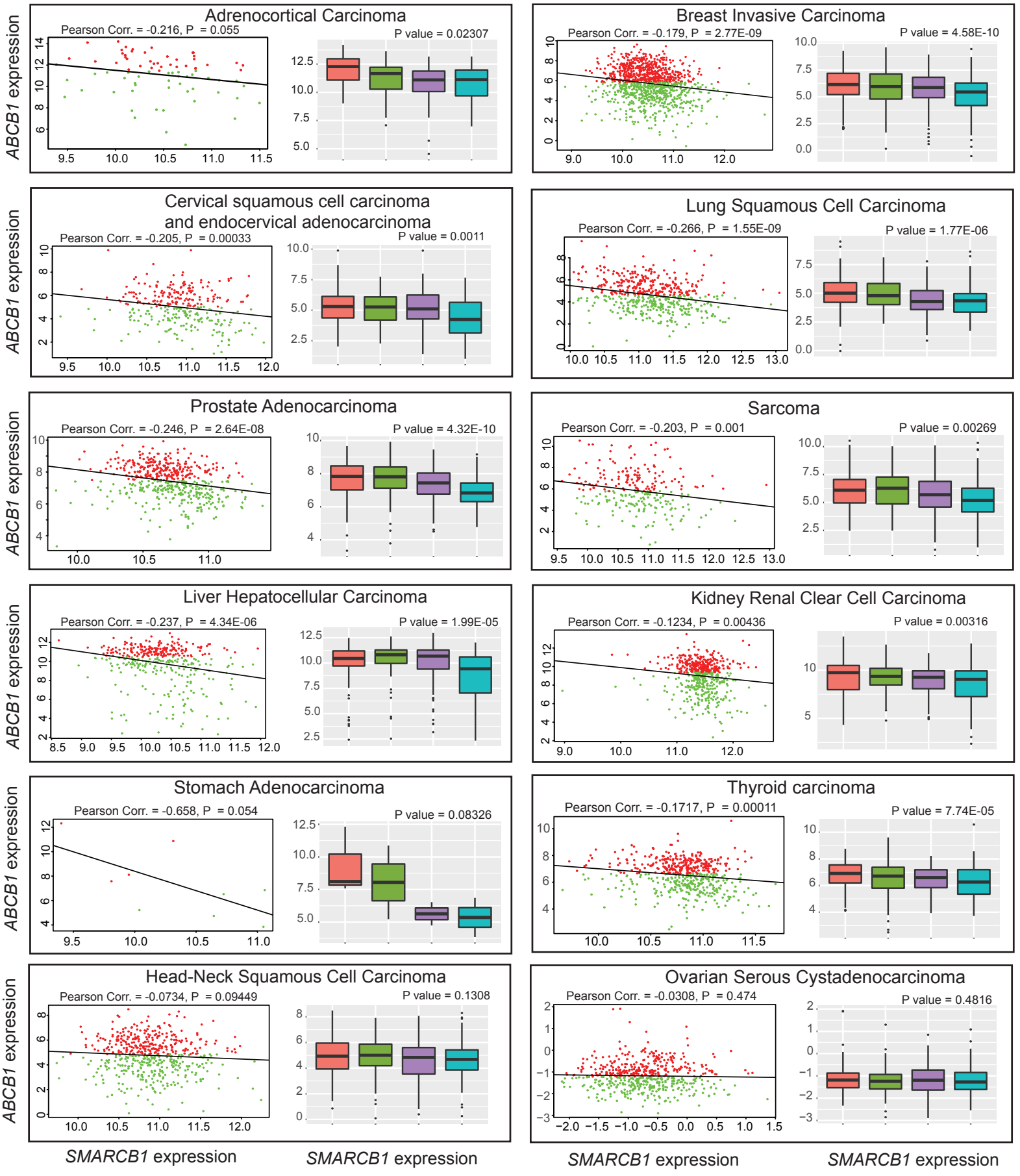

Supplementary Figure 2. Correlation between ABCB1 and *SMARCB1* mRNA expression levels across multiple human cancers represented in the TCGA database. For each cancer, the left graph shows the linear correlation, along with the Pearson Correlation Coefficient and *p*-value, between *ABCB1* expression and *SMARCB1* expression. Red dots are samples with *ABCB1* expression below the median value and green dots denote samples with *ABCB1* expression above the median value. Box and whisker plots on the right show *ABCB1* expression (y-axis) in samples from the four consecutive quartiles of *SMARCB1* expression, with the p-value testing statistical significance for the difference in *ABCB1* expression between samples in the top and bottom quartile of *SMARCB1* expression. In all graphs, *ABCB1* expression is plotted in the y-axis and *SMARCB1* expression on the x-axis.

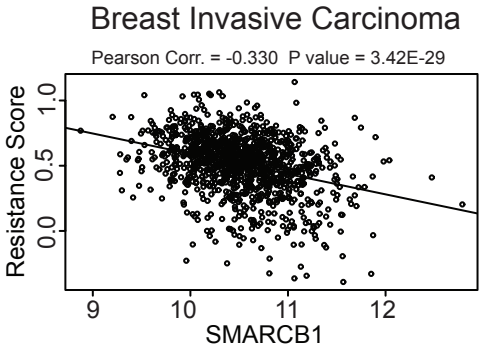
Breast Invasive Carcinoma
Pearson Corr. = -0.330 P value = 3.42E-29
Resistance Score
SMARCB1

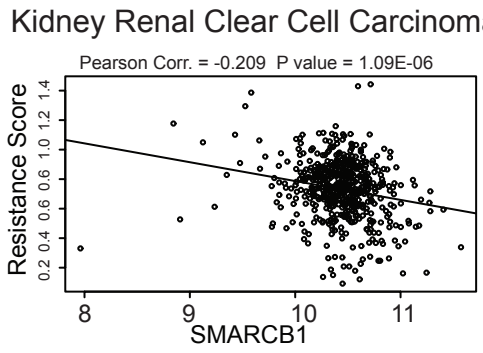
Kidney Renal Clear Cell Carcinoma
Pearson Corr. = -0.209 P value = 1.09E-06
Resistance Score
SMARCB1

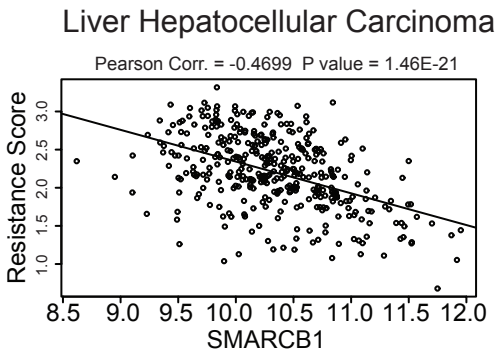
Liver Hepatocellular Carcinoma
Pearson Corr. = -0.4699 P value = 1.46E-21
Resistance Score
SMARCB1

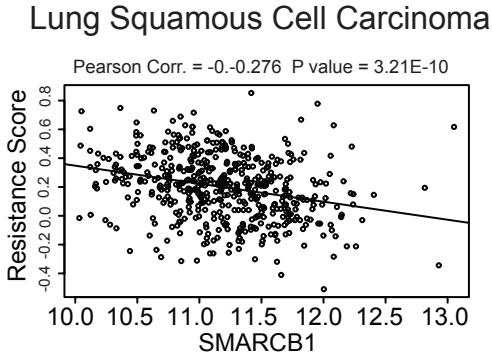
Lung Squamous Cell Carcinoma
Pearson Corr. = -0.-0.276 P value = 3.21E-10
Resistance Score
SMARCB1

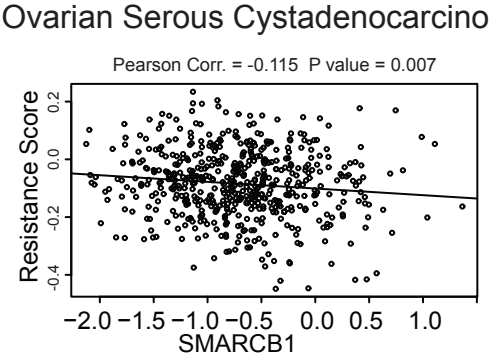
Ovarian Serous Cystadenocarcinoma
Pearson Corr. = -0.115 P value = 0.007
Resistance Score
SMARCB1

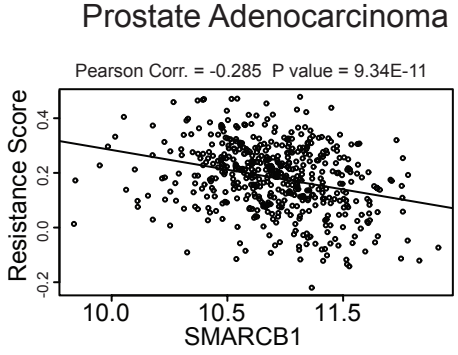
Prostate Adenocarcinoma
Pearson Corr. = -0.285 P value = 9.34E-11
Resistance Score
SMARCB1

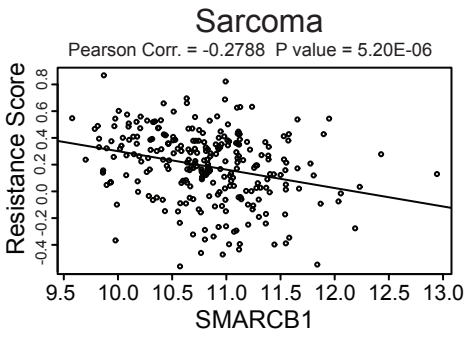
Sarcoma
Pearson Corr. = -0.2788 P value = 5.20E-06
Resistance Score
SMARCB1

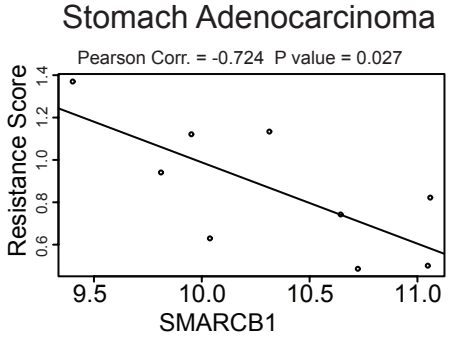
Stomach Adenocarcinoma
Pearson Corr. = -0.724 P value = 0.027
Resistance Score
SMARCB1

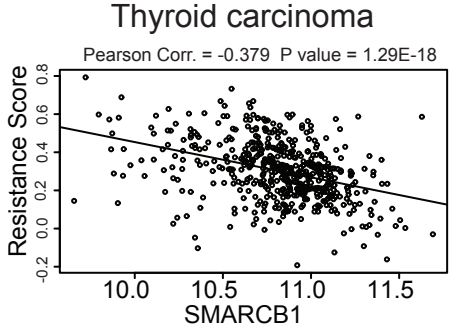
Thyroid carcinoma
Pearson Corr. = -0.379 P value = 1.29E-18
Resistance Score
SMARCB1

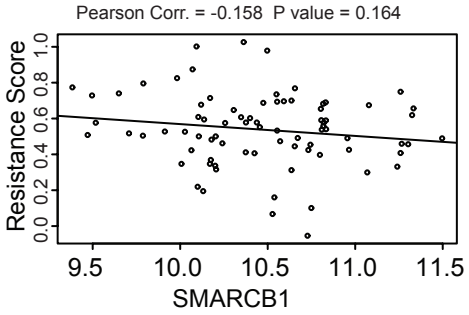
Adrenocortical Carcinoma
Pearson Corr. = -0.158 P value = 0.164
Resistance Score
SMARCB1

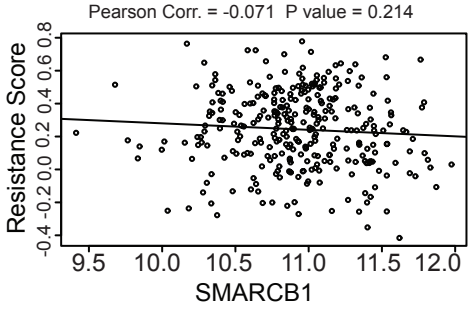
Cervical squamous cell carcinoma
and endocervical adenocarcinoma
Pearson Corr. = -0.071 P value = 0.214
Resistance Score
SMARCB1

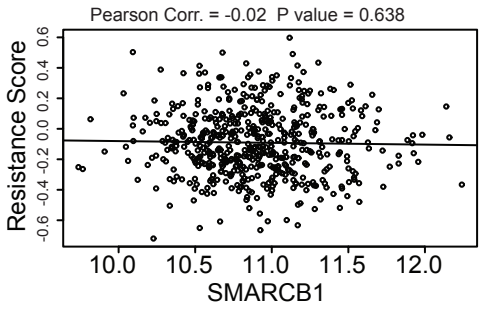
Head-Neck Squamous
Cell Carcinoma
Pearson Corr. = -0.02 P value = 0.638
Resistance Score
SMARCB1

Supplementary Figure 3. Correlation between *SMARCB1* expression and doxorubicin resistance across multiple human cancers represented in the TCGA database. Each plot shows the linear correlation between SMARCB1 expression levels (x-axis) and a Dox resistance score (y-axis), which is derived from a gene-expression signature of Dox resistance (see Supplementary Materials and Methods for derivation of the score), along with the Pearson Correlation Coefficient and *p*-value. The negative correlation coefficients suggest that lower SMARCB1 expression levels are associated with increased Dox resistance. Statistically significant correlations were not seen in the three cancers shown on the bottom row.

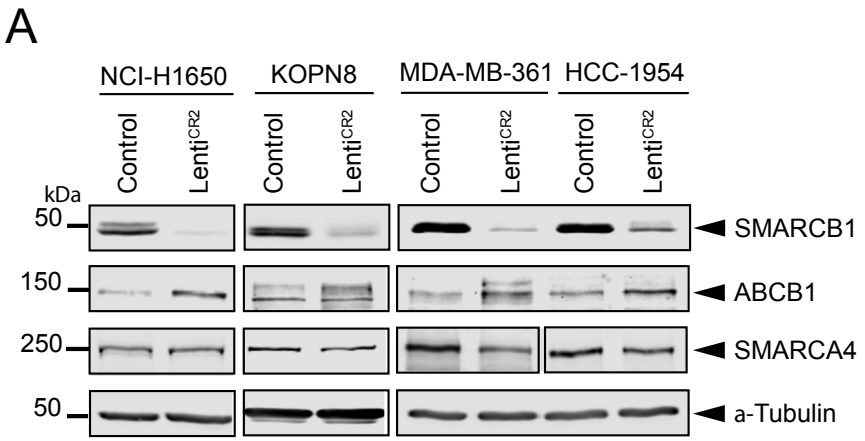
A
NCI-H1650
KOPN8
MDA-MB-361
HCC-1954
Control
Lenti^CR2
kDa
50
150
250
50
SMARCB1
ABCB1
SMARCA4
a-Tubulin

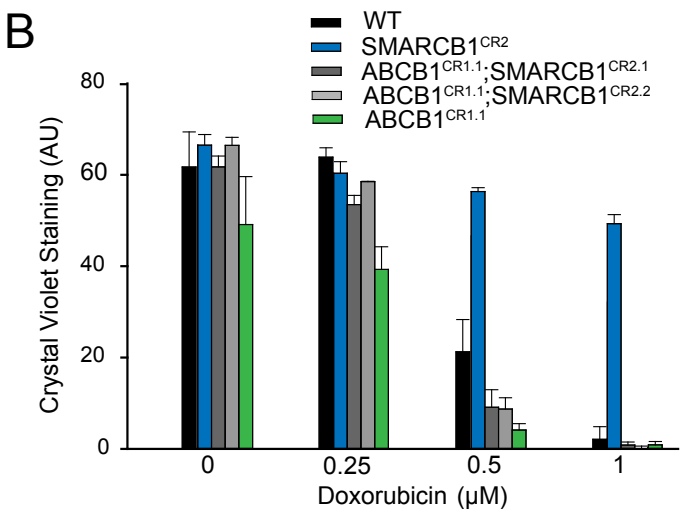
B
WT
SMARCB1^CR2
ABCB1^CR1.1;SMARCB1^CR2.1
ABCB1^CR1.1;SMARCB1^CR2.2
ABCB1^CR1.1
Crystal Violet Staining (AU)
0
20
40
60
80
0
0.25
0.5
1
Doxorubicin (μM)

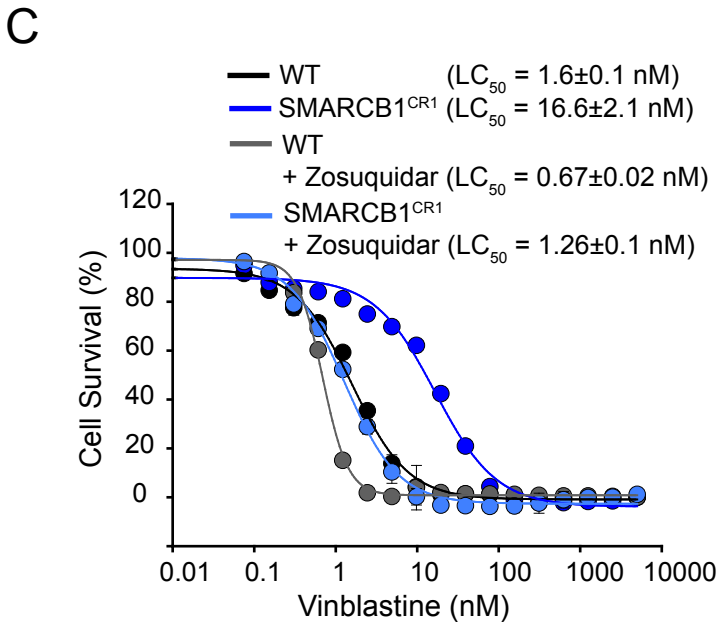
C
WT (LC50 = 1.6±0.1 nM)
SMARCB1^CR1 (LC50 = 16.6±2.1 nM)
WT
+ Zosuquidar (LC50 = 0.67±0.02 nM)
SMARCB1^CR1
+ Zosuquidar (LC50 = 1.26±0.1 nM)
Cell Survival (%)
0
20
40
60
80
100
120
0.01
0.1
1
10
100
1000
10000
Vinblastine (nM)

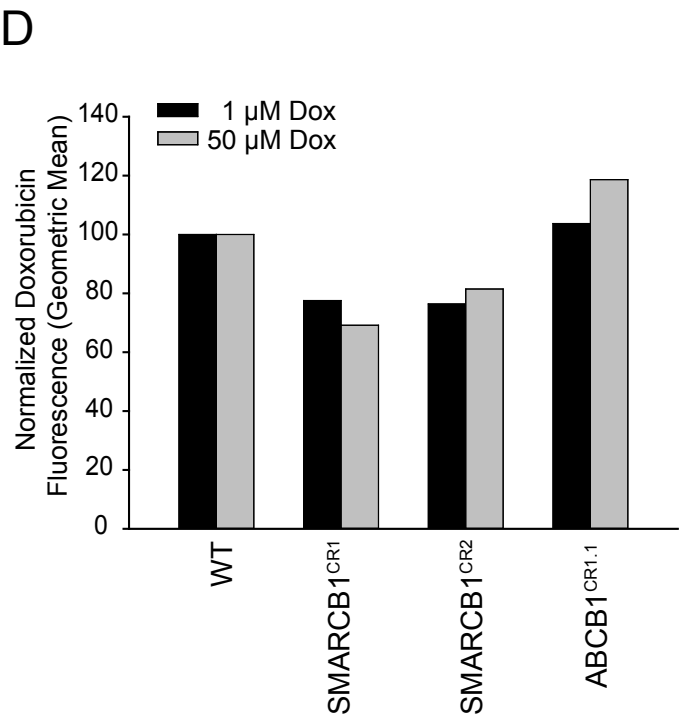
D
1 μM Dox
50 μM Dox
Normalized Doxorubicin Fluorescence (Geometric Mean)
0
20
40
60
80
100
120
140
WT
SMARCB1^CR1
SMARCB1^CR2
ABCB1^CR1.1

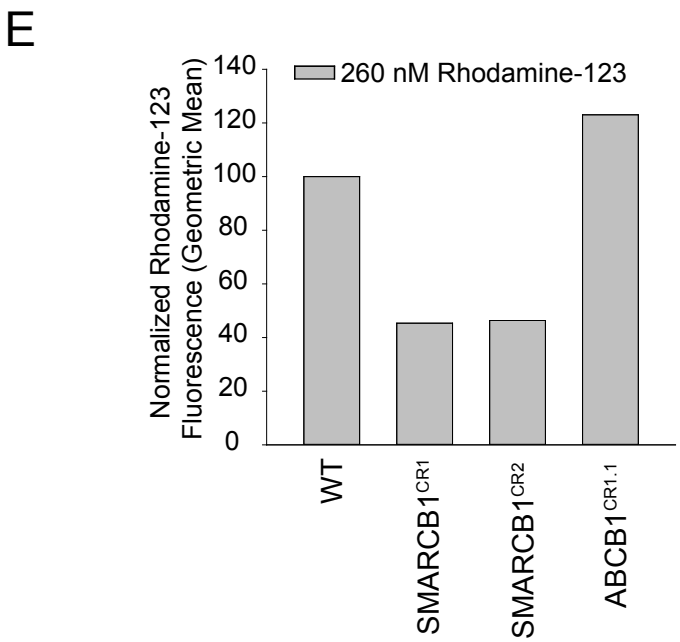
E
260 nM Rhodamine-123
Normalized Rhodamine-123 Fluorescence (Geometric Mean)
0
20
40
60
80
100
120
140
WT
SMARCB1^CR1
SMARCB1^CR2
ABCB1^CR1.1

Supplementary Figure 4. SMARCB1 loss leads to ABCB1 upregulation, drug resistance and reduced Dox accumulation. (**A**) Immunoblotting was used to measure SMARCB1 and ABCB1 protein levels in several cancer cell lines infected with a control lentivirus or a lentivirus carrying a validated gRNA (LentiCR2) targeted to the *SMARCB1* locus. (**B**) Quantification of data from Figure 5E showing the survival of single and double mutant cell lines that were treated with a transient 2 hrs pulse of Dox, followed by drug removal and growth for 10 d. (**C**) Vinblastine LC_{50} was measured using an MTT assay (96 h) in cell lines lacking SMARCB1 in the absence or presence of Zosuquidar (100 nM). Zosuquidar reversed Vinblastine resistance in SMARCB1 null cells. Accumulation of Dox (**D**) or Rhodamine-123 (**E**) was determined by Fluorescence Activated Cell Sorting (FACS) after incubation of the indicated cell lines for 2 hrs with Dox and 1 hr with Rhodamine-123. The geometric mean of the fluorescence depicted is calculated from 19,315±295 cells for the Rhodamine-123 experiment, 15,635±2168 cells for the 1 μM Dox experiment and 24,948±5233 cells for the 50 μM Dox experiment. Error bars denote S.D. (*n*=3 in **B**; *n*=4 in **C**).

Supplementary Figure 5

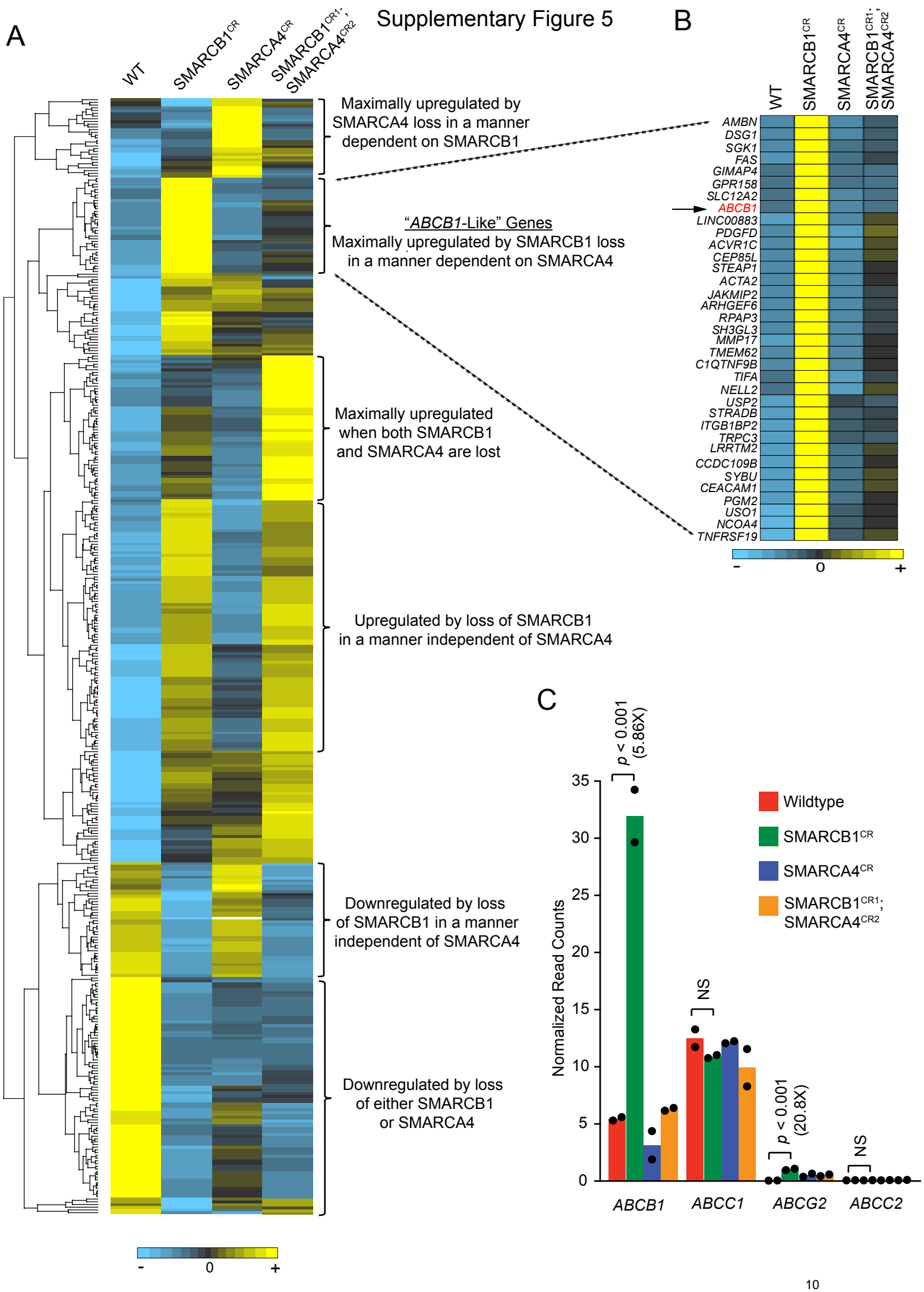

Supplementary Figure 5. Hierarchical clustering reveals multiple classes of genes that are differentially expressed in WT Hap1 cells compared to Hap1 cells lacking SMARCB1. (**A**) The heat map depicts the relative expression of each gene (based on an average derived from two replicates) across WT cells, cells lacking either SMARCB1 or SMARCA4 alone, and cells lacking both genes. Only genes that were either upregulated (≥ 2.0 fold) or downregulated (≤ 0.5 fold) in the WT vs. $SMARCB1^{CR}$ comparison, passed a FDR corrected *p*-value of threshold of <0.001 and were represented by >1,000 total reads were included in this analysis. Descriptions are provided for distinct sets of genes based on their transcriptional response to the depletion of SMARCA4, SMARCB1 or both proteins. Genes that most closely resemble the pattern of ABCB1 expression across the 4 cell lines are denoted “ABCB1-like” genes and shown in more detail in (**B**). (**C**) Expression of the four ABC-family transporters most closely associated with Dox resistance in human cancer in HAP1 cells lacking SMARCB1, SMARCA4 or both proteins. Black dots depict normalized RNAseq read counts from two different cell lines, and the bar is drawn at the mean value. Numbers above the bars depict the fold-change and associated *p*-value for the comparison between WT cells and cells lacking SMARCB1. For ABCC1 and ABCC2, no difference in expression was observed between the two cell lines (NS=non-significant).